

Propulsion and Steering of Helical Magnetic Microrobots using Two Synchronized Rotating Dipole Fields in Three-Dimensional Space

Abdelrahman Hosney*, Anke Klingner*, Sarthak Misra^{†§} and Islam S. M. Khalil*

Abstract— We control the motion of helical microrobots with average diameter of $500\ \mu\text{m}$ in two-dimensional (2D) and three-dimensional (3D) spaces using two synchronized rotating dipole fields. The utilization of the two synchronized dipole fields not only increases the magnetic torque exerted on the magnetic dipole of the helical microrobot but also eliminates the magnetic field gradients along its lateral directions. Our finite element simulations and experimental results show that the utilization of two rotating dipole fields increases the magnetic field by 100%, as opposed to single rotating magnetic field. In addition, we show that the magnetic field gradient within the workspace of the microrobot is eliminated. Therefore, the lateral oscillations of the helical microrobot are mitigated within the center of two rotating dipole fields, and hence the motion of the microrobot is stabilized inside tubes with relatively large inner diameters, as opposed to the diameter of the helical microrobot. This strategy allows the microrobot to compensate for gravity and swim in 3D space inside water reservoirs at an average speed of 0.25 body lengths per second. In addition, closed-loop motion control of the helical microrobot is achieved in 2D space at an average speed of 2 mm/s and maximum steady-state error of $100\ \mu\text{m}$.

I. INTRODUCTION

Control of helical microrobots [1], [2], [3], [4] using magnetic systems with open-configuration has at least two advantages over magnetic control using closed-configurations of electromagnetic coils [5]. First, the closed-configurations have limited workspace since they cannot be scaled up to the size of *in vivo* devices [6]. Second, the closed-configuration of electromagnetic coils makes it difficult to incorporate a clinical imaging modality during *in vivo* experiments [7], [8]. These challenges can be overcome by the control of helical microrobots using electromagnetic system with open-configurations that have been demonstrated by Fountain *et al.* [9] and Mahoney *et al.* [10], [11]. The helical propulsion of magnetic robots using single rotating dipole field is usually achieved inside tubes and lumens with inner diameters that are slightly larger than the outer diameter of the helical microrobots [12]. The drift caused by the magnetic field gradients and forces due to gravity cause motion instability during the helical propulsion of these microrobots. Mahoney *et al.* [13] have proposed a gravity

This work was supported by funds from the German University in Cairo and the DAAD-BMBF funding project.

*The authors are affiliated with the German University in Cairo, New Cairo City 11835, Egypt. islam.shoukry@guc.edu.eg

[†]Sarthak Misra is affiliated with the Department of Biomechanical Engineering, MIRA-Institute for Biomedical Technology and Technical Medicine, University of Twente, Enschede, The Netherlands. s.misra@utwente.nl

[§]Department of Biomedical Engineering, University of Groningen and University Medical Centre Groningen, The Netherlands.

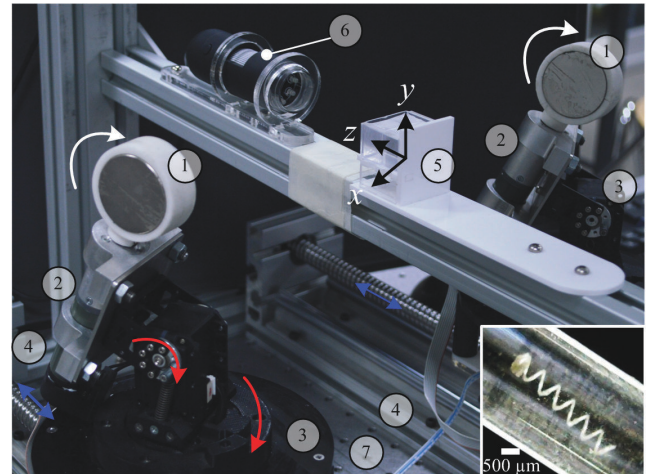


Fig. 1. A magnetic-based robotic system for the wireless motion control of a helical microrobot (inset) in three-dimensional space using two rotating dipole fields. The system consists of two rotating permanent magnets ① using two DC motors ②. The motors are fixed on two robotics bases ③ with 2 degrees-of-freedom and are provided with linear motion along z -axis using two linear motion stages ④. The motion control in three-dimensional space is done inside a water container ⑤. The motion of the helical microrobot is determined using two cameras ⑥ and our feature tracking algorithm. The system is mounted on a vibration isolation table ⑦. The black, red and blue arrows indicate the motion of the motors, robotic bases, and linear motion stages, respectively. The inset shows the helical propulsion of a microrobot at an average speed of $483\ \mu\text{m/s}$ without lateral oscillations.

compensation algorithm to compensate for the forces due to gravity by orienting the helical microrobot and controlling its angular speed. It has been qualitatively demonstrated in [14] that the helical microrobots exhibit undesirable lateral oscillations in their motion inside tubes with relatively large inner diameter under the influence of single rotating dipole field. These undesirable oscillations can be mitigated by using two synchronized rotating dipole fields.

In this work, we study the influence of two rotating dipole fields on the resultant magnetic force and magnetic torque exerted on a helical microrobot (Fig. 1). We compensate for the forces that cause drift and instability, i.e., gradient forces along the lateral directions of the microrobot and forces due to gravity. The gradient forces are compensated by using two synchronized rotating dipole fields, whereas the gravitational forces are compensated by controlling the angular velocity and the direction of the helical microrobot (based on the gravity compensation algorithm presented by Mahoney *et al.* [13]). This study is done on a magnetic-based robotic system with two rotating dipole fields. The

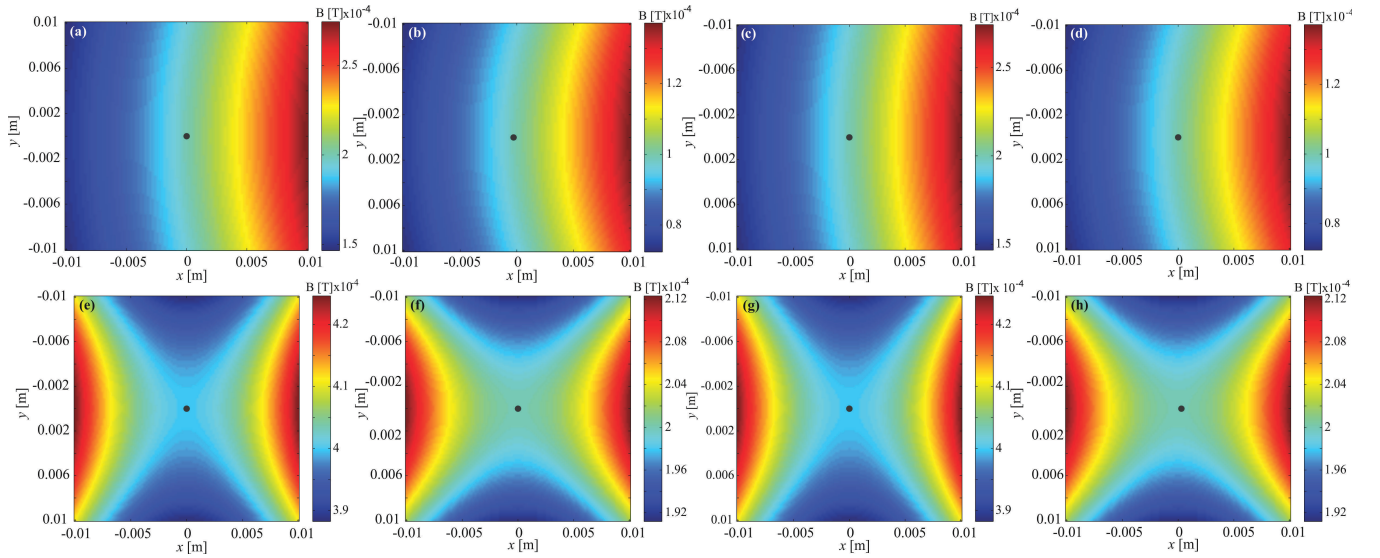


Fig. 2. Simulation of the magnetic field exerted on a helical microrobot using single rotating dipole field (top) and two rotating dipole fields (bottom). The magnetic field magnitude is calculated at 4 representative orientations of the permanent magnets, i.e., 0° , 90° , 180° , and 270° with respect to x -axis (from left to right). The magnetic field ($\mathbf{B}(\mathbf{P})$) exerts a magnetic torque on the dipole (\mathbf{m}) of the helical microrobot (small gray circle). The magnetic field generated using the two rotating dipole fields at the center of the workspace ($x = 0$) is 100% greater than the magnitude of the magnetic field generated using single dipole field. The magnetic field gradient almost vanishes at, $x = 0$, for the two rotating dipole fields. The magnetic dipole moment of the rotating dipole field and the distance to the center of the reservoir are, $m_m=1$ C.m and $l=0.1$ m, respectively. The finite element model is created using Matlab (MathWorks, Natick, Massachusetts, U.S.A.). (a) The magnetic field at, $x = 0$, is calculated to be 0.2 mT for orientation of 0° of single dipole field. (b) The magnetic field at, $x = 0$, is calculated to be 0.1 mT for orientation of 90° of single dipole field. (c) The magnetic field at, $x = 0$, is calculated to be 0.2 mT for orientation of 180° of single dipole field. (d) The magnetic field at, $x = 0$, is calculated to be 0.1 mT for orientation of 270° of single dipole field. (e) The magnetic field at, $x = 0$, is calculated to be 0.4 mT for orientation of 0° of two dipole fields. (f) The magnetic field at, $x = 0$, is calculated to be 0.2 mT for orientation of 90° of two dipole fields. (g) The magnetic field at, $x = 0$, is calculated to be 0.4 mT for orientation of 180° of two dipole fields. (h) The magnetic field at, $x = 0$, is calculated to be 0.2 mT for orientation of 270° of two dipole fields.

utilization of two rotating dipole fields allows us to increase the magnetic torque exerted on the magnetic dipole of the helical microrobot while eliminating the components of the magnetic field gradients that causes lateral oscillations. This strategy allows us to control the motion of the helical microrobot inside tubes with large inner diameter compared to the diameter of the helical microrobot in three-dimensional (3D) space. In addition, we achieve closed-loop motion control of the helical microrobots under microscopic guidance in two-dimensional (2D) space without lateral oscillations.

The remainder of this paper is organized as follows: Section II provides a finite element (FE) model of our magnetic-based robotic system and simulation results of the elimination of the magnetic field gradients along x - and y -axis. Descriptions of the magnetic-based robotic system are included in Section III. In addition, point-to-point motion control in 2D space and motion control of time varying trajectories with gravity compensation in 3D space are provided. Finally, Section IV concludes and provides directions for future work.

II. THE PROPULSION USING TWO SYNCHRONIZED ROTATING DIPOLE FIELDS

The propulsion of the helical microrobot using single rotating dipole field results in motion instability due to the magnetic field gradients (helical propulsion using Helmholtz coil electromagnets limits the workspace and is difficult to be scaled up). The single rotating dipole field configuration

provides undesirable magnetic force components along x - and y -axis (Fig. 2). We develop an FE model of the two rotating dipole fields. The magnetic field gradients are calculated numerically for 4 representative orientations of the rotating dipole fields (0° , 90° , 180° , and 270°). The electromagnetic configuration shown in Fig. 1 allows us to generate a strong periodic external magnetic field ($\mathbf{B}(\mathbf{P}, t)$) that is given by

$$\mathbf{B}(\mathbf{P}, t + \tau) = \mathbf{B}(\mathbf{P}, t), \quad (1)$$

where t and τ are the time and the periodic time, respectively, and are related to the angular frequency (ω) using, $\omega = \frac{2\pi}{\tau}$. Further, \mathbf{P} is the position of the microrobot. The magnetic field is produced by one or two rotating permanent magnets. The helical microrobot consists of a permanent magnet with magnetic moment (\mathbf{m}) attached to a helical structure, as shown in Fig. 1. The axis of the helix and the magnetic moment are perpendicular. The magnetic field gradient results in a magnetic force ($\mathbf{F} = (\mathbf{m} \cdot \nabla)\mathbf{B}$) and a magnetic torque ($\mathbf{T} = \mathbf{m} \times \mathbf{B}$) on the helical microrobot. Our aim is to minimize the force on the helical microrobot to stabilize its motion and maximize the magnetic torque exerted on its magnetic dipole.

In our FE model, the center of the coordinate system is at the center of the reservoir that contains the microrobot. One or two magnets are placed at $(l, 0, 0)$ and $(\pm l, 0, 0)$, respectively, where l is the distance between the rotating dipole field (the permanent magnet) and the center of the reservoir. The length and magnetic strength of the permanent

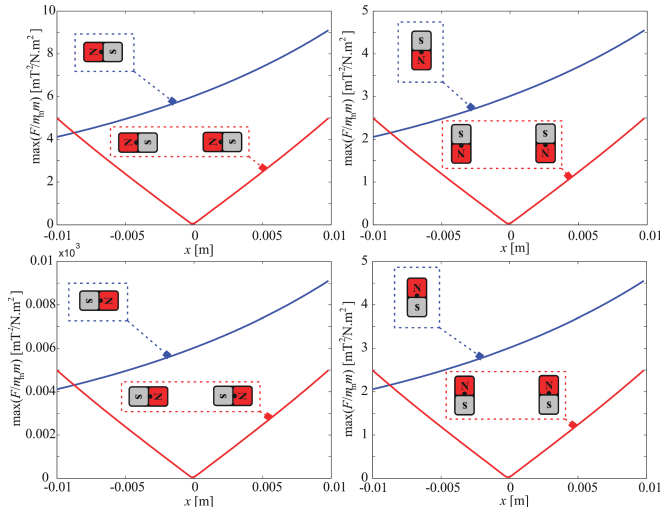


Fig. 3. The calculated ratio of the magnetic force and the product of the magnetic dipole moments of the permanent magnets and the helical microrobot ($\frac{F}{m_p m}$). m_m and m are the magnitudes of magnetic dipole moments of the permanent magnet and helical microrobot, respectively. This ratio is calculated for 4 orientations of the rotating permanent magnets (single and two dipole fields). The blue and red lines represent the magnetic field gradients of the single and two dipole fields, respectively. The magnetic field gradient vanishes within the center of the workspace ($x = 0$) for the two dipole fields, whereas non-zero magnetic field gradient exists for the single dipole field throughout a rotation of 360° of the rotating dipole fields. The magnetic force is calculated using (3) and (4). The insets indicate schematic representations of the configurations of the permanent magnets.

magnets are 20 mm and 387.5 mT (on the face of the magnet). The angle of the magnet is measured between the north pole of the permanent magnet and the positive x -axis. The resultant magnetic fields for the single and two rotating dipole fields at 4 representative orientations of the permanent magnets are calculated. Figs. 2(a), (b), (c), and (d) show the calculated magnetic fields for orientations of 0° , 90° , 180° , and 270° , respectively (single rotating dipole field). This simulation result shows that the magnetic field is non-uniform within the center of the reservoir. Therefore, magnetic force components along x - and y -axis are generated. These forces causes motion instability when the helical microrobot is controlled inside tubes or container that are relatively larger than the diameter of the microrobot. The magnetic fields generated using the configuration of two synchronized dipole fields are shown in Figs. 2(e), (f), (g), and (h) for orientations of 0° , 90° , 180° , and 270° , respectively. The FE simulation indicates that the magnetic field is uniform within the center of the workspace. Therefore, the magnetic field gradients vanish at the position of the helical microrobot throughout a rotation of 360° of the rotating dipole fields.

The magnetic field gradients are calculated and used to simulate the magnetic forces on the magnetic dipole of the microrobot. The permanent magnet is modeled as a dipole with magnetic dipole moment (\mathbf{m}_m). The angle of the magnet is measured between the north pole of the magnet and the positive x -axis. Therefore, the magnetic moment

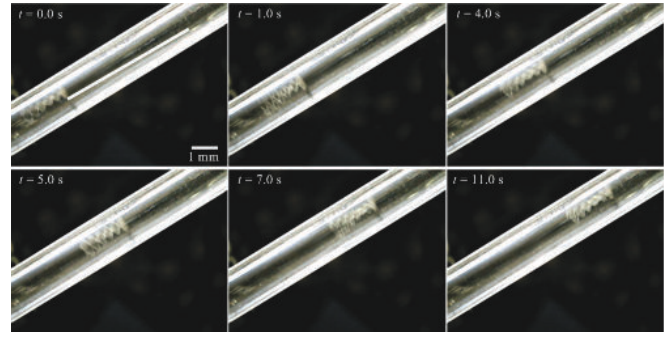


Fig. 4. A representative motion control result of a helical microrobot with diameter of $500 \mu\text{m}$ inside a tube under the influence of two rotating dipole fields. The helical microrobot swims at an average speed of $483 \mu\text{m/s}$ for rotating dipole field of 8 Hz. The two synchronized rotating dipole fields allow the helical microrobot to rotate and swim with minimal lateral oscillations. Please refer to the accompanying video that demonstrates the helical propulsion of a microrobot using two rotating dipole fields.

vector is given by

$$\mathbf{m}_m = \begin{bmatrix} m_m \cos \alpha & m_m \sin \alpha & 0 \end{bmatrix}, \quad (2)$$

where m_m is the magnitude of the magnetic dipole moment of the permanent magnet, and α is the angle between the magnetic dipole moment and the positive x -axis. At, $\alpha = 0^\circ$, the magnet at $(l, 0, 0)$ points with the south pole towards the reservoir and the magnet at $(-l, 0, 0)$ points with the north pole towards the reservoir. The magnetic field is given by

$$\mathbf{B}(\mathbf{P}) = \frac{\mu_o}{4\pi} \left(\frac{3\mathbf{P}(\mathbf{m}_m \cdot \mathbf{P})}{|\mathbf{P}|^5} - \frac{\mathbf{m}_m}{|\mathbf{P}|^3} \right). \quad (3)$$

In (3), μ_0 is the permeability constant. We use (3) to calculate the magnetic force (\mathbf{F}) exerted on the magnetic dipole of the microrobot using

$$\mathbf{F} = m \left(\cos \theta \sin \delta \frac{d}{dx} + \sin \theta \sin \delta \frac{d}{dy} + \cos \delta \frac{d}{dz} \right) \mathbf{B}, \quad (4)$$

where θ and δ are the angles between the axis of the helical microrobot and the x - and z -axis, respectively. Further, m is the magnetic dipole moment of the helical microrobot. We use (4) to calculate the magnetic force exerted on the magnetic dipole moment of the helical microrobots for the single and double rotating dipole fields. Fig. 3 shows the calculated magnetic force at 4 representative orientations

TABLE I

SPECIFICATION OF THE MAGNETIC-BASED ROBOTIC SYSTEM THAT CONSISTS OF LINEAR MOTION STAGES AND ROBOTIC BASES (LIGHT GRAY), AND DIMENSIONS OF THE HELICAL MICROROBOT.

Parameter	Value	Parameter	Value
Range [mm]	85	Pitch (stage) [mm]	1.0
Velocity [mm/s]	39	Increment [μm]	50
Load [N]	38.2	Push/pull force [N]	0.37
Material	Al	Dimensions [mm^3]	$20 \times 20 \times 20$
Diameter [μm]	400	Length [mm]	2 – 3
Pitch [μm]	500	Number of turns	5

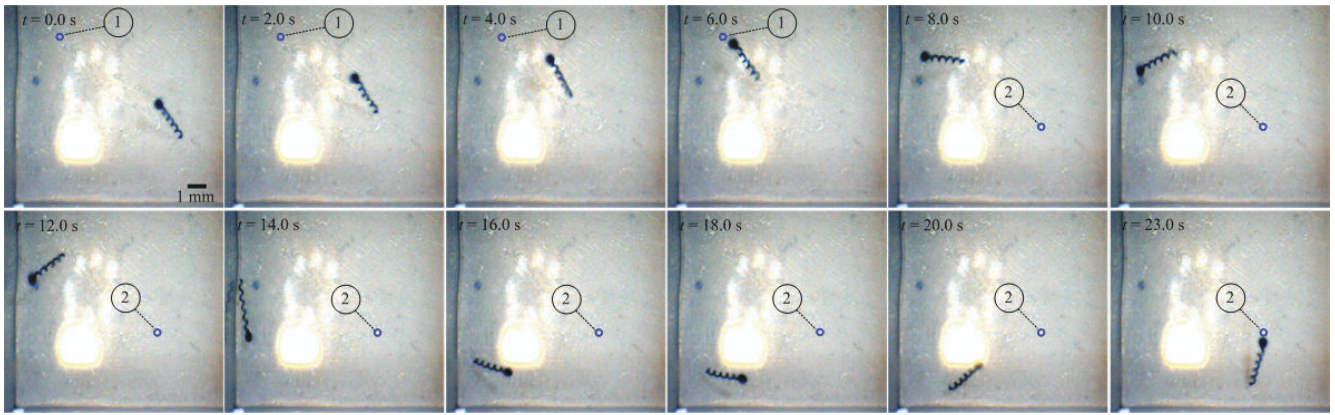


Fig. 5. A representative motion control result of a helical microrobot with a diameter of $500 \mu\text{m}$ inside a water reservoir in two dimensional (2D) space. The microrobot swims at an average speed of $875 \mu\text{m/s}$ under the influence of two synchronized rotating dipole fields. The frequency of the rotating dipole fields is 8 Hz. The angle between the axis of the helical microrobot and z -axis is 20° . This angle does not generate enough propulsive force component to compensate for the force due to gravity. The small blue circles indicate two reference positions. The rotating dipole fields allow the microrobot to orient towards the reference position and achieve helical propulsion towards them. Please refer to the accompanying video that demonstrates the helical propulsion of a microrobot using two rotating dipole fields in 2D space.

of the rotating permanent magnets. There exists a pulling magnetic force components on the helical microrobot that is driven using single rotating dipole field, whereas these force components vanishes when the microrobot is driven using the two synchronized dipole fields.

Fig. 3 provides the calculated maximum force ($\frac{F}{m_m m}$) since the magnitude of magnetic force (F) is proportional to the dipole moment of the microrobot (m) and that of the rotating permanent magnets (m_m). The maximum force decreases with distance from the single permanent magnet at, $l = 10 \text{ cm}$. Along y -direction, the maximum force is approximately constant from a single permanent magnet. For two permanent magnets the force is zero at, $x = 0$ and $y = 0$, and increases linearly with the distance from this point. Along x -axis, the maximum force increases faster than in y -direction as the ratio reaches a value of $5 \text{ mT}^2/\text{N}\cdot\text{m}^2$, at $x = 1 \text{ cm}$, and only $2.3 \text{ mT}^2/\text{N}\cdot\text{m}^2$, at $y = 1 \text{ cm}$. The maximum force is smaller for two permanent magnets than for single permanent magnet. Therefore, a helical microrobot at the center of the rotating dipole fields is subjected to a minimal magnetic force. In addition, our simulation results shows that the magnetic fields generated using two dipole fields are 100% greater than the fields generated using single dipole field (Fig. 2). Therefore, the microrobot is subjected to higher magnetic torque to improve the helical propulsion and lower gradient to decrease the drift compared to helical propulsion using single dipole field.

We observe that the motion of the helical microrobot is stabilized because of the elimination of the magnetic force components along the lateral directions of the microrobot, as opposed to propulsion using single dipole field. Fig. 4 provides a representative motion control experiment of a helical microrobot using two rotating dipole field. In this representative experiment the rotating dipole field has a frequency of 8 Hz, and the average speed of the helical microrobot is calculated to be $483 \mu\text{m/s}$. This experiment is repeated and we observe consistency in the elimination

of the lateral oscillations of the microrobot, as opposed to propulsion using single dipole field. Please refer to the accompanying video that demonstrates the helical propulsion of a microrobot using two rotating dipole fields.

III. MOTION CONTROL OF THE HELICAL MICROROBOT IN 2D AND 3D SPACES

Motion control of the helical microrobots is achieved using two rotating dipole fields in 2D and 3D spaces inside water reservoir. The magnetic fields are generated using a magnetic-based robotic system.

A. Magnetic-Based Robotic System

Our magnetic-based robotic system consists of two linear motion stages. Their motion is synchronized and controlled using an Arduino control board (Arduino Mega 2560, Arduino, Memphis, Tennessee, USA). Each motion stage carries a robotic base (Cyton Gamma 300, Robai, Cambridge, USA) with 3 degrees-of-freedom. The end-effector of each robotic base holds a DC motor (Maxon 47.022.022-00.19-189 DC Motor, Maxon Motors, Sachseln, Switzerland) that rotates a permanent magnet (N40 Neodymium, Amazing Magnets LLC, California, U.S.A) with outer diameter and thickness of 38 mm and 20 mm, respectively. This system is mounted on a tuned damped optical table (M-ST-UT2-58-12, Newport, California, U.S.A) and the motion of the helical microrobot is observed using a Sony XCD-X710 (Sony Corporation, Tokyo, Japan) FireWire camera in xz -plane and a digital camera in yz -plane. The helical microrobots are fabricated using helical springs with diameter of $500 \mu\text{m}$ and length of 2 mm to 3 mm. The helical angle and pitch of the helical structure are 60° and $400 \mu\text{m}$, respectively. A magnetic dipole moment is added to the helical structure by attaching a permanent magnet (N40 Neodymium, Amazing Magnets LLC, California, U.S.A) with a cubic structure (edge length of $500 \mu\text{m}$) to one end of the helical structure. Table I provides the specification of the magnetic-based robotic system and the helical microrobot.

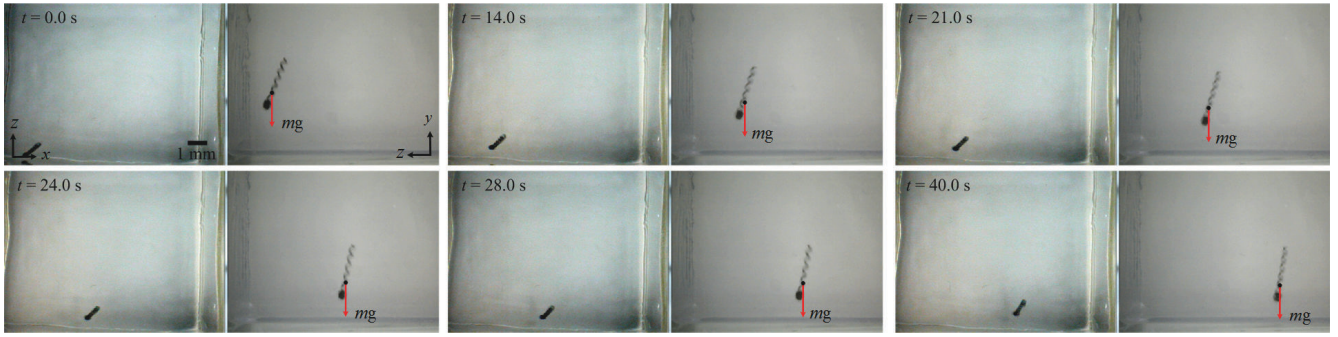


Fig. 6. A representative motion control of a helical microrobot in three-dimensional (3D) space under the influence of two synchronized rotating dipole fields. The microrobot swims and compensates gradient forces and the force due to gravity (mg), m is the mass of the microrobot and g is the acceleration due to gravity. The helical microrobot swims at an average speed of $196.1 \mu\text{m/s}$ and rotates at frequency of 8 Hz. We observe that the helical microrobot compensates for gravity and moves upward at, $\delta=63^\circ$. Please refer to the accompanying video that demonstrates the helical propulsion of a microrobot using two rotating dipole fields in 3D space.

B. Propulsion and Steering using Two Rotating Fields

The rotating magnetic fields are used to direct and move the helical microrobot towards a reference position within a 2D workspace. The two rotating permanent magnets allow the microrobot to rotate and move forward, whereas the robotic bases change the orientation of the permanent magnets to direct the helical microrobot towards the reference positions. This level of control is done by maintaining the axis of the permanent magnets parallel to the longitudinal axis of the microrobot. The reference position (\mathbf{P}_{ref}) and the orientation (θ) of the helical microrobot are used to calculate the orientation error (e_θ) using

$$e_\theta = \theta_{\text{ref}} - \theta, \quad (5)$$

where θ_{ref} is the reference orientation that orients the microrobot toward the reference position. Further, θ is the orientation of the helical microrobot with respect to the cartesian coordinates of the system (Fig. 1). This angular position is determined by tracking the ends of the helical microrobot using our feature tracking algorithm [14], [15]. Therefore, the orientation of the helical microrobot is given by

$$\theta = \tan^{-1} \left(\frac{y_2 - y_1}{x_2 - x_1} \right), \quad (6)$$

where $\mathbf{P}_1 = [x_1 \ y_1]^T$ and $\mathbf{P}_2 = [x_2 \ y_2]^T$ are the positions of the first and second end points of the helical microrobot, respectively. A proportional control system is designed based on the position error (5), and is used to control the orientation of the permanent magnets. The DC motors rotates the permanent magnets at a constant angular velocity (8 Hz), while the robotic bases change the orientation of the DC motors based on the position tracking error (5).

C. Motion Control Experimental Results

Helical propulsion and steering are achieved in 2D and 3D spaces under the influence of the two synchronized rotating dipole fields. Fig. 5 shows a representative motion control towards two reference positions. The average swimming speed is calculated to be $875 \mu\text{m/s}$, at frequency of 8 Hz.

The angle between the axis of the helical microrobot and y -axis is adjusted to be 20° . Therefore, the force due to gravity is not compensated in this experiment, and the helical microrobot does not have motion along y -axis (upward). Therefore, we observe that one end of the helical microrobot is in contact with the bottom of the reservoir. However, the helical microrobot moves towards two reference positions and can be localized within their vicinities. Please refer to the accompanying video that demonstrates the helical propulsion of a microrobot using two synchronized dipole fields in 2D space.

We increase the angle between the axis of the helical microrobot and the z -axis gradually to observe the orientation that allows the microrobot to compensate for gravity [13]. At, $\delta=63^\circ$, the helical microrobot compensates for gravity and moves upwards, as shown in Fig. 6. However, the average swimming speed is calculated to be $196.1 \mu\text{m/s}$ at frequency of 8 Hz (compensation of the forces due to gravity decreases the propulsion force of swimming). Please refer to the accompanying video that demonstrates the helical propulsion of a microrobot using two synchronized dipole fields in 3D space.

Tracking of a circular trajectory in 3D is also achieved using our two synchronized rotating dipole fields, as shown in Fig. 7. This tracking is done by compensating the gradient forces and the forces due gravity by the utilization of two dipole fields and controlling the angle of the helical microrobot, respectively. In this representative experiment, the helical microrobot swims at an average speed of $171 \mu\text{m/s}$, at frequency of 8 Hz of the rotating dipole fields. The gradient forces are mitigated, and this allows the helical microrobot to swim along the circular trajectory in the xz -plane. In addition, the force due to gravity is eliminated by the helical propulsion as shown in the yz -plane. Please refer to the accompanying video that demonstrates the helical propulsion of a microrobot using two rotating dipole fields in 3D space.

IV. CONCLUSIONS AND FUTURE WORK

We study the helical propulsion of a microrobot under the influence of single and two synchronized rotating dipole

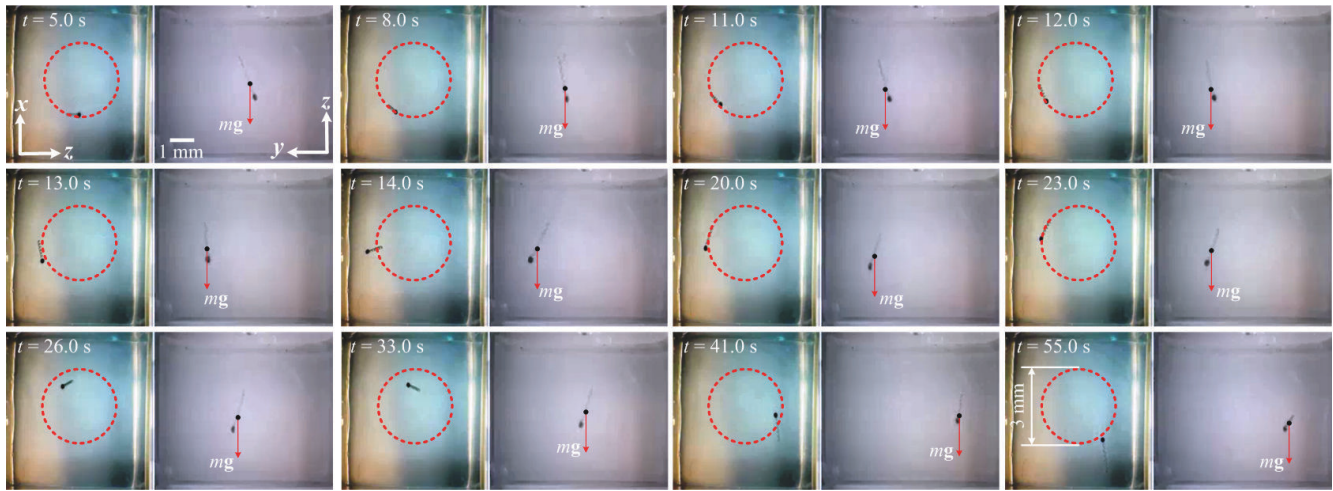


Fig. 7. A representative motion control result of the helical microrobot in three-dimensional (3D) space. The helical microrobot is following a circular trajectory in xz -plane with a diameter of 3 mm. The force (mg) due to gravity is compensated by the helical propulsion of the microrobot (yz -plane), where m is the mass of the microrobot and g is the acceleration due to gravity. The average speed of the helical microrobot is calculated to be $171 \mu\text{m/s}$, at frequency of 8 Hz of the rotating dipole fields. Please refer to the accompanying video that demonstrates the helical propulsion of a microrobot using two rotating dipole fields in 3D space.

fields. Our FE simulations and experimental results show that the magnetic torque exerted on the magnetic dipole of the microrobot is increased by 100% using two synchronized dipole field, whereas the magnetic force components along the lateral directions of the microrobot almost vanish within the center of the configuration of the two rotating dipole fields. This configuration allows the helical robot to eliminate the gradient forces and forces due to gravity. We show that our helical microrobot can be controlled in 3D space at an average speed of $171 \mu\text{m/s}$, at frequency of 8 Hz.

As part of future work, the helical microrobots will be controlled inside microfluidic channel against and along the flowing streams of a simulated body fluid and will be used in clearing blood clots *in vitro*. In addition, our magnetic-based electromagnetic system will be adapted to integrate an ultrasound imaging modality to provide visual feedback to the control system. Moreover, we will use the helical propulsion using two synchronized dipole fields to achieve micromanipulation and microassembly of non-magnetic microobjects in 2D and 3D spaces.

REFERENCES

- [1] K. E. Peyer, L. Zhang, B. J. Nelson, "Bio-inspired magnetic swimming microrobots for biomedical applications", *Nanoscale*, vol. 5, no. 4, pp. 1259-1272, November 2012.
- [2] D. J. Bell, S. Leutenegger, K. M. Hammar, L. X. Dong, B. J. Nelson, "Flagella-like propulsion for microrobots using a magnetic nanocoil and a rotating electromagnetic field", in *Proceedings of the IEEE International Conference on Robotics and Automation (ICRA)*, pp. 1128-1133, April 2007.
- [3] J. J. Abbott, K. E. Peyer, L. Dong, and B. Nelson, "How should microrobots swim?" *The International Journal of Robotics Research*, vol. 28, no. 11-12, pp. 1434-1447, July 2009.
- [4] E. M. Purcell, "Life at low reynolds number," *American J. Physics*, vol. 45, no. 1, pp. 3-11, June 1977.
- [5] M. P. Kummer, J. J. Abbott, B. E. Kartochovil, R. Borer, A. Sengul, and B. J. Nelson, "OctoMag: an electromagnetic system for 5-DOF wireless micromanipulation," *IEEE Transactions on Robotics*, vol. 26, no. 6, pp. 1006-1017, December 2010.
- [6] B. J. Nelson, I. K. Kaliakatsos, and J. J. Abbott, "Microrobots for minimally invasive medicine," *Annual Review of Biomedical Engineering*, vol. 12, pp. 55-85, April 2010.
- [7] S. Martel, O. Felfoul, J.-B. Mathieu, A. Chanu, S. Tamaz, M. Mohammadi, M. Mankiewicz, and N. Tabatabaei, "MRI-based medical nanorobotic platform for the control of magnetic nanoparticles and flagellated bacteria for target interventions in human capillaries," *International Journal of Robotics Research*, vol. 28, no. 9, pp. 1169-1182, September 2009.
- [8] I. S. M. Khalil, P. Ferreira, R. Eleutério, C. L. de Korte, and S. Misra, "Magnetic-Based closed-loop control of paramagnetic microparticles using ultrasound feedback," in *Proceedings of the IEEE International Conference on Robotics and Automation (ICRA)*, pp. 3807-3812, Hong Kong, China, June 2014.
- [9] T. W. R. Fountain, P. V. Kailat, and J. J. Abbott, "Wireless control of magnetic helical microrobots using a rotating-permanent-magnet manipulator," in *Proceedings of the IEEE International Conference on Robotics and Automation (ICRA)*, pp. 576-581, Alaska, USA, May 2010.
- [10] A. W. Mahoney, D. L. Cowan, K. M. Miller, and J. J. Abbott, "Control of untethered magnetically actuated tools using a rotating permanent magnet in any position," in *Proceedings of the IEEE International Conference on Robotics and Automation (ICRA)*, pp. 3375-3380, Minnesota, USA, May 2012.
- [11] A. W. Mahoney and J. J. Abbott, "Control of untethered magnetically actuated tools with localization uncertainty using a rotating permanent magnet," in *Proceedings of the IEEE RAS/EMBS International Conference on Biomedical Robotics and Biomechatronics (BioRob)*, pp. 1632-1637, Rome, Italy, June 2012.
- [12] A. W. Mahoney and J. J. Abbott, "Managing magnetic force applied to a magnetic device by a rotating dipole field," *Applied Physics Letters*, 99, September 2011.
- [13] A. W. Mahoney, J. C. Sarrazin, E. Bamberg, and J. J. Abbott, "Velocity control with gravity compensation for magnetic helical microswimmers," *Advanced Robotics*, vol. 28, no. 8, pp. 1007-1028, April 2012.
- [14] M. E. Alshafeei, A. Hosney, A. Klingner, S. Misra, and I. S. M. Khalil, "Magnetic-Based motion control of a helical robot using two synchronized rotating dipole fields," in *Proceedings of the IEEE RAS/EMBS International Conference on Biomedical Robotics and Biomechatronics (BioRob)*, pp. 151-156, São Paulo, Brazil, August 2014.
- [15] I. S. M. Khalil, J. D. Keuning, L. Abelmann, and S. Misra, "Wireless magnetic-based control of paramagnetic microparticles," in *Proceedings of the IEEE RAS/EMBS International Conference on Biomedical Robotics and Biomechatronics (BioRob)*, pp. 460-466, Rome, Italy, June 2012.